International Journal of Adhesion & Adhesives 143 (2025) 104160

Contents lists available at ScienceDirect

International Journal of Adhesion and Adhesives

journal homepage: www.elsevier.com/locate/ijadhadh

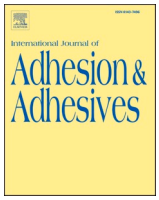

Environmental effects on the fractographic analysis of Mode I delamination on secondary and co-bonded composite adhesive joints

Núbia N.A. Silveira [a,b], Camila B.G. Brito [a,c], Geraldo M. Cândido [a], Maurício V. Donadon [a], Rita C.M. Sales-Contini [a,d,*]

[a] Aeronautics Institute of Technology, Praça Marechal do Ar Eduardo Gomes, Vila das Acácias CEP, 12228-900, São José dos Campos/SP, Brazil
[b] University of Twente, Drienerlolaan 5, Enschede, 7522 NB, the Netherlands
[c] Delft University of Technology (TU Delft), Kluyverweg 1, 2629 HS, Delft, the Netherlands
[d] Technologycal College of São José dos Campos, Professor Jessen Vidal, Centro Paula Souza, Av Cesare Mansueto Giulio Lattes, 1350 Distrito Eugênio de Melo, 12247-014, São José dos Campos/SP, Brazil

ARTICLE INFO

Keywords:
Fractography
Mode I
Co-bonded
Secondary bonded
Delamination
Environmental conditioning

ABSTRACT

Adhesive bonding technologies for thermoset polymer composites have been used in marine, automotive, construction and aerospace industries due to their superior mechanical behaviour (high strength-to-weight ratio, damage tolerance and fatigue resistance) compared to conventional joining methods. The main disadvantage of this joining technology is its susceptibility to delamination due to disbonding during use. Loading conditions, adhesive type, ageing effects and lack of inspection procedures are just some of the elements that affect the overall structural performance of the composite joint during the manufacturing process. A deeper understanding of how these elements affect joint behaviour is required to improve joint performance and design. This work provides a comparative fractographic analysis for two different joint types: co-bonded (CB) and secondary bonded (SB) joints, under Mode I delamination at elevated temperature and high humidity conditions. Fractographic analysis was used to compare the two joint technologies and explain the differences in toughness values and fracture behaviour, revealing crack propagation mechanisms in composite joints. While the CB and SB joints have comparable fracture toughness (G_{IC}) values, different fracture characteristics and bonding methods can discern these two bonding technologies, indicating that SB joints are more susceptible to environmental conditioning.

1. Introduction

The traditional mechanical fastening method for joining aeronautical structures is gradually being replaced by adhesive bonding. Adhesive bonding has gained popularity due to its ability to distribute loads more evenly, improve aerodynamics by eliminating protruding fasteners, and reduce weight by eliminating drilled holes to install the fasteners. Adhesive bonding involves using a bonding agent applied between two surfaces to join them together. This method relies on the bonding agent's ability to provide strength and the right force distribution, increasing the joint durability [1]. However, during cruise conditions, these structures are exposed to adverse environmental conditions. Understanding how environmental factors such as temperature and moisture affect the mechanical performance of adhesive bonding in composite aeronautical structures is crucial for ensuring the structural integrity and reliability of aircraft components [2].

Moisture absorption in the context of composite materials must take into account the potential swelling that can worsen delamination. This swelling contributes to increasing interlaminar stresses, thus promoting delamination growth within the composite structure. The presence of moisture can also catalyse the development of microcracks in composite materials, compromising their overall integrity and structural stability in the long term. Moreover, moisture absorbed in the composite material can induce dimensional alterations, leading to warping or distortion in the structure. These changes can impact the mechanical properties and performance under load. Consequently, misalignments between layers may arise from these dimensional changes, creating stress concentrations that heighten the risk of delamination in the composite material

* Corresponding author. Aeronautics Institute of Technology, Praça Marechal do Ar Eduardo Gomes, Vila das Acácias CEP, 12228-900, São José dos Campos/SP, Brazil.
E-mail address: rita.sales@fatec.sp.gov.br (R.C.M. Sales-Contini).

https://doi.org/10.1016/j.ijadhadh.2025.104160
Received 29 November 2024; Received in revised form 9 June 2025; Accepted 15 September 2025
Available online 25 September 2025

and structural failure [3,4]. Furthermore, the interaction between moisture absorption and temperature variations can expedite chemical reactions in the composite material, potentially compromising the bonding between layers and increasing susceptibility to delamination [5].

Temperature fluctuation is a variable that can impact the structural strength of the composite. Elevated temperatures can speed up the spread of moisture in the composite, worsening the abovementioned problems and possibly causing a quicker deterioration process that can greatly decrease the lifespan of the composite part and weaken its capacity to endure mechanical pressures, ultimately creating safety hazards in structural uses [6]. Therefore, the combination of moisture absorption with elevated temperature plays a crucial role in the interlaminar fracture toughness of adhesive joints in polymer composite structures. Some studies have shown that the translaminar fracture toughness of carbon/epoxy composites increases with temperature, especially under wet conditions, indicating a significant rise in toughness with moisture saturation [7–11]. In recent years, researchers have extensively studied the interlaminar fracture toughness of composite joints exposed to extreme environmental conditions and correlated the mechanical results with SEM analysis. Abdel Monsef et al. [12] observed that the conditioning environment temperature was identified as a significant factor affecting the Mode II fracture toughness of the joints. Specimens conditioned at higher temperatures experienced the most significant reduction in fracture toughness, indicating the sensitivity of the joint's performance to temperature variations. Brito et al. [2] studied the Mode I interlaminar fracture toughness of co-cured and co-bonded CFRP joints, comparing as-received and conditioned specimens, and observed that co-bonded joints are more susceptible to the changes in environmental conditioning when compared with the co-cured ones.

Advanced imaging techniques, like scanning electron microscopy (SEM), are crucial for understanding failure mechanisms and the performance of bonded structures by examining fracture surfaces. SEM analysis can give further insights into the delamination process by revealing internal structures and defects of different Modes of load and environmental conditions. SEM results studied by Olander et al. [13] indicated that subtle interactions and variations at the bond interface/interphase region could significantly influence the performance of the bonded joint. By characterising these regions at the nanoscale level, the study provided insights into process-dependent variables and potentially expanded the operating limits for these bonded systems. Silveira et al. [14] investigated the Mode II interlaminar fracture toughness of CFRP joints of two adhesive composite joints: co-bonded and secondary bonded. They concluded that environmental conditioning reduced the fracture toughness of both joints. However, the CB joint showed an overall better performance than the SB joint due to its manufacturing process, which is based on chemical bonding between the adhesive and the substrate, providing robust adhesion mechanisms as proven by the analysis of fracture aspects using the SEM technique.

Therefore, the main objective of this work is to characterise the failure aspects observed in composite joints manufactured by co-bonding (CB) and secondary bonding (SB) technologies, subjected to Mode I static load and conditioned at elevated temperature and high humidity. All these aspects are explained through fractographic analysis, the environmental conditioning effects on each type of joint. The fractographic analysis provides valuable insights into the crack propagation mechanisms and failure modes exhibited by the composite joints under Mode I static delamination, shedding light on the structural integrity of the bonded interfaces.

2. Methodology

2.1. Joint manufacturing processes

Two types of joints - co-bonded (CB) and secondary-bonded (SB) - were examined during this study. Toray® T800/3900-2C unidirectional carbon/epoxy with a thermoplastic dispersed-particle interlayer was the material utilised for the prepreg, called the interleaf region. Loctite® EA9695 adhesive was utilised to create the junction. For CB joint technology, one of the laminates was autoclave-cured before use. The curing process followed the instructions in the manufacturer's technical data sheet [15].

i) A full vacuum was applied to the part.
ii) 655 kPa of pressure was applied.
iii) The vacuum bag was vented when the autoclave pressure reached 138 kPa.
iv) A heating rate of 1.7 °C/min was used until 177 °C was reached.
v) The laminate remained at 177 °C for 120–180 min.
vi) The cooling process occurred at a maximum rate of 2.78 °C/min until 60 °C was reached.

A peel-ply layer is used to protect the composite surface during cure and to improve the roughness on the composite's surface once removed. Once cured, the peel-ply layer was removed. Loctite® EA9695 adhesive was applied, and the second, still uncured, plate was placed on top of it. A polyester net was used in the middle plane of the adhesive to keep its thickness constant. To produce an initial crack, a Teflon® sheet was placed between the two plates, at the adhesive's plane. The stack cured-plate-adhesive-uncured plate was then autoclaved using the same curing process at 177 °C. For the SB joint technology, the two laminates were cured separately using the same curing process as for the CB laminate, with a peel ply layer on both plates. After removing the peel-ply layer, both laminates were bonded together using Loctite® EA9695 adhesive (again with the polyester net and the Teflon® film placed at the adhesive's plane). To cure the adhesive, the stack cured-plate-adhesive-cured plate was autoclaved at 177 °C. After the final cure, once the joints were established, the specimens were cut using ASTM D5528 [16] to describe specified dimensions (170x20 × 5 mm).

2.2. Moisture absorption and water diffusion measurements

Six specimens of each bonding technology were conditioned at 80 °C, 90 % humidity, and atmospheric pressure in the Vötsch Industrietechnik® conditioning chamber VC3 7100. These specimens were named for *ETW*, standing for "elevated temperature wet". All mentions to ETW made from now on refer to tests done on specimens that underwent these conditions. The specimen's weight was assessed every day until the seventh day and then every 15 days until the specimen's water absorption stabilised. According to ASTM D5229/D5229M standard [17], the difference in percentage between two successive measurements should have values less than 0.020 % to verify this stabilisation. An analytical Mettler Toledo® Al204 Class 1 scale was used to weigh the specimens. The Fickian approach was used to calculate the water diffusion rate in the specimens. Weight increase over time was addressed by this strategy [18]. By using the ASTM 5229 standard, the diffusion percentages are derived from the weight growth as a function of the square root of the period, according to Equation (1) [17]:

$$D_z = \pi\left(\frac{h}{4M_m}\right)^2\left(\frac{M_2 - M_1}{\sqrt{t_2} - \sqrt{t_1}}\right)^2 \quad (1)$$

where: D_z is the diffusion speed; h is the mean specimen thickness, M_m is the effective moisture balance content (%), M_2-M_1 slope of the moisture absorption plot on the initial and $\sqrt{t_2}$-$\sqrt{t_1}$ linear curve the time, $\sqrt{\text{seconds}}^{-1}$.

2.3. Fracture toughness tests

The six standardised specimens (170 x 20 × 5 mm) were prepared as described in Section 2.1. An insert of Teflon® film with dimensions of 60 mm was used to simulate an initial crack. The specimen surface was

cleaned using laboratory-grade acetone (99.5 %, Merck®). To apply the opening forces during the Mode I delamination test according to the ASTM D5528 standard [16], polished aluminium loading blocks (20x15 × 15 mm) were bonded to each side of the specimens where the Teflon film was present. The specimens were not pre-cracked before testing. One of the specimen's edges was polished with acetone and spray-painted white, on which fine lines of 1 mm increments for the first 5 mm of growth from the delamination front and then in 5 mm increments for a further 20 mm were scribed with a height gauge to aid the observation of the delamination front using a CCD camera positioned on one side of the specimens. A photograph of the DCB test setup is presented in Fig. 1.

The Mode I delamination test was conducted using an Instron® 5500R machine with a 2 kN load cell and a displacement rate of 1 mm/min. A thermal chamber coupled to the testing machine was used to carry out the high-temperature test (80 °C) with a relative humidity of 50 % (see Fig. 1). The load and displacement were recorded using Instron software.

The Mode I interlaminar fracture toughness (G_{IC}) was determined according to ASTM D5528 [16] and calculated using Equation (3):

$$G_{Ic} = \frac{3P\delta}{2b(a+|\Delta|)}F \tag{3}$$

Where P is the load, δ is the load direction displacement, b is the specimen width, a is the delamination length after the Teflon® insert, Δ is the delamination front rotation correction, and F is the correction factor that accounts for large displacements and end block effects. The value of Δ was determined from the modulus of the intercept on the delamination length axis in the graph of the cube root of compliance, $C^{1}/^{3}$ versus delamination length, a.

In this study, visual observation (VIS) was employed as a method to follow the crack propagation. The G_{IC} was calculated at the first point at which the operator could identify the beginning of delamination. To enhance visualisation of the delamination front (specifically the crack tip), a CCD camera was positioned next to the specimens.

The advancement of the delamination front in response to applied load and displacement was documented using a crack marker that was activated whenever the crack crossed the marked vertical lines scribed on the spray-painted white face of the specimens.

In composite material joints, particularly heterogeneous ones composed of reinforcement, matrix and adhesive [2,3,19], stick-slip behaviour can appear during mode I delamination testing [16]. The stick-slip behaviour observed in the load-displacement curves is characterized by minimum and maximum fracture toughness values associated with minimum (P_{min}) and maximum (P_{max}) load levels that define a single stick-slip cycle. The data reduction scheme adopted in this paper to obtain the Mode I fracture toughness for all cases where the stick-slip was observed, is based on the maximum load level (P_{max}) measured for each stick-slip cycle so that, at P_{max} the crack grows rapidly and rests at P_{min}. The load is then further increased until a new P_{max} is reached, leading to further crack growth associated with a subsequent stick-slip cycle.

2.4. Fractographic analysis

After the Mode I test, one specimen of each kind of joint was selected based on the best fracture toughness values for further evaluation in the SEM. A 45 × 20 mm tiny specimen was cut, and a 5 nm-thick gold layer was applied over the specimen's fracture surface using a Quorum Q150R ES sputter coater. The fractographic analysis was carried out using two Scanning Electron Microscopes: Quanta 250 and a VEGA3 XMU TESCAN. Secondary electron analyses with an acceleration energy of 5–10 keV, a beam intensity of 9–10, and a working distance of 14–16 mm were used to create the images.

ASTM D5573 [21] was utilised to categorise the failure Modes observed in the specimen fracture surfaces, where a few failure Modes are possible.

- Adhesive failure: when failure happens between the adhesive-adherent interface
- Cohesive failure: when a crack propagates within the adhesive layer itself.
- Thin-layer cohesive failure: if a cohesive failure occurs near the adhesive-adherent interface
- Fibre tear failure: when a crack propagates in the adherent, being identified by the presence of the reinforcing fibres on both sides of the rupture.

The results presented in this work were compared with those reported by Brito's work [2,3] and Silveira's work [19].

3. Results and discussion

3.1. Moisture absorption of CB and SB joints

For better monitoring, a percentage of moisture absorbed at time t versus root time curve was generated as the weighting sessions happened. This procedure allowed the evaluation of how much more time the samples would still need until stabilisation was reached. When

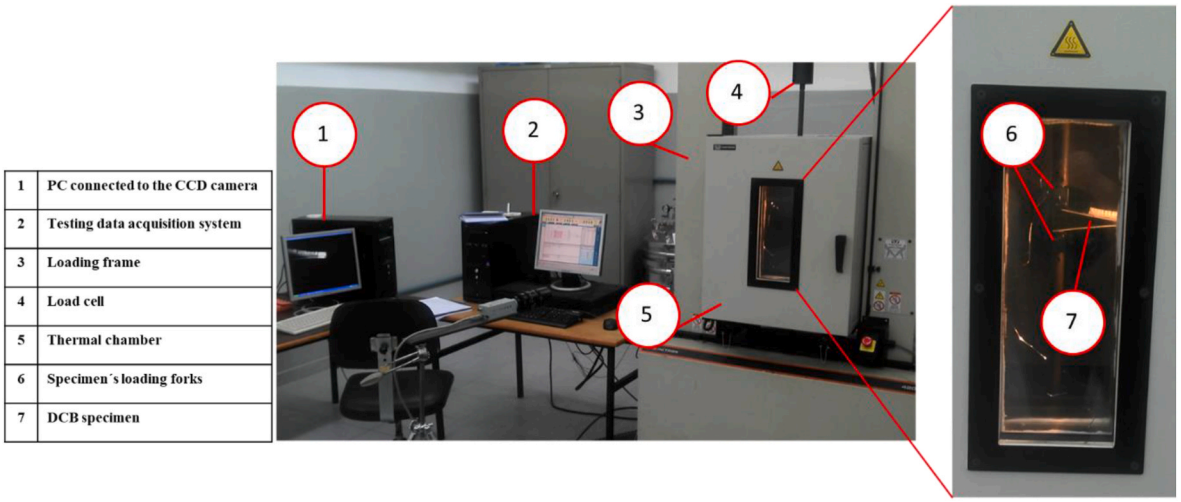

1	PC connected to the CCD camera
2	Testing data acquisition system
3	Loading frame
4	Load cell
5	Thermal chamber
6	Specimen´s loading forks
7	DCB specimen

Fig. 1. Experimental setup used to characterise Mode I interlaminar fracture toughness.

the curve growth started tending to a plateau during the biweekly-interval measurements, the weighting was restarted to be done weekly.

Fig. 2 shows two different curves of absorption, one for each joint technology analysed, during the three months they have been stored in the climatic chamber. It is interesting to notice that there is a small but perceptible difference between the amount of moisture soaked by the laminates of each bonding technique. It is intuitive to think that the adhesive has influenced the moisture uptake process [22], leading to a greater percentage of humidity intake in the laminates that have the adhesive as part of the bond, as is the case of co-bonding and secondary bonding, as can be seen in Fig. 2.

It can be noticed that the water diffusion in SB joints has lower values ($8.966x10^{-9}$ mm^2/s) than those obtained for the CB joints ($9.506x10^{-9}$ mm^2/s), indicating that there is a barrier for the water ingress in these joints. This behaviour was expected because the SB joints were submitted to cure at 177 °C and a post-curing process at the same temperature (177 °C). In addition, these sequential processes promote an increase in the crosslink density [23,24], making it a more difficult process for the water ingress [25,26].

Crosslinking is a chemical process that happens when a low molecular weight resin is combined with a hardener. Typically, this reaction takes place at temperatures above room temperature and may necessitate the presence of a catalyst. The curing begins with the elongation and branching of polymer chains. As the reaction progresses, the molecular weight and viscosity increase. Ultimately, these chains interconnect to create a vast, interlinked network with a higher density of crosslinks and tighter packing of the polymer chains, which reduces the spaces between them [27]. The curing conditions, such as temperature and pressure, applied in autoclave equipment to speed up the reaction in polymeric composites also aid in the densification of the material. This reduction in voids and free volume between the polymer chains makes it harder for water to penetrate the matrix [28].

Regarding the coefficient of diffusion, it was shown that CB specimens presented a value slightly higher than the one obtained for SB specimens. This result was attributed to the differences in manufacturing processes of each technology. Since both laminates in SB technology are already cured during the cure process of the adhesive and the pre-cured laminates, it is believed that this post-cure contributes to an increase in the crosslink density of the laminates. This higher crosslink density is believed to be the cause for the slower water intake process, quantified by the lower coefficient of diffusion reported for SB samples [13].

3.2. Failure aspects of ETW CB joints

Fig. 3 shows the Mode I load versus displacement curve of ETW CB specimens and its direct correspondence to the pattern observed in the ETW CB fracture surface. The stick-slip behaviour (characterised by consecutive gradual increases in load followed by abrupt drops) in ETW specimens is less pronounced than that observed in the as-received specimens, as shown in Brito's work [2] (referred to as RTA, standing

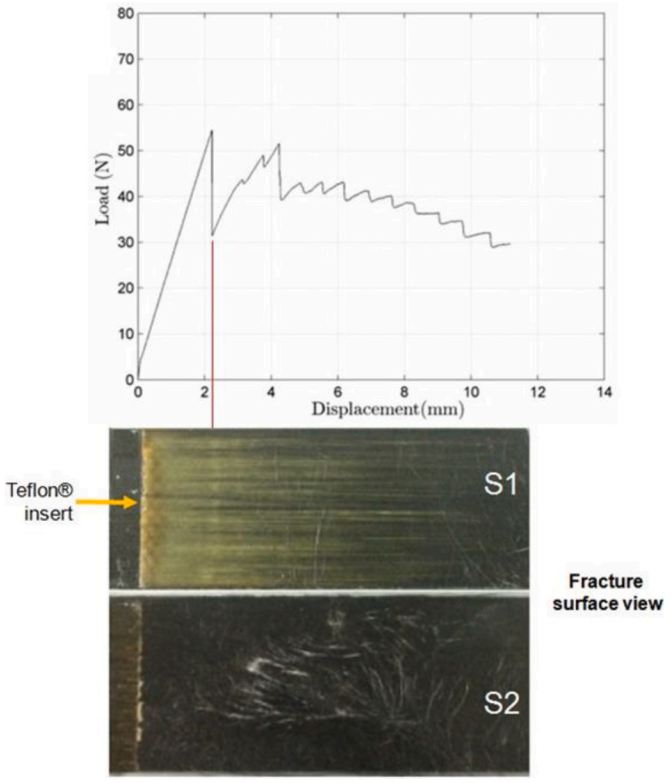

Fig. 3. Load versus displacement curve of CB specimens related to the pattern observed in their fracture surface in ETW condition under Mode I load.

for "room temperature and ambient humidity"). The fracture toughness value is also lower than the one reported for as-received specimens, where the G_{IC} value was 0.235 ± 0.048 N/mm versus 0.217 ± 0.022 N/mm for ETW, which is 7.66 % lower than that for as-received specimens.

Analysing the image obtained by optical microscopy, Silveira et al. [19] observed that the RTA specimen fracture surface showed two failure Modes: a cohesive failure in the middle of the adhesive layer and the light fibre tear at the edge of the laminate, followed by a failure Mode dominated by fibre tear during delamination propagation. In contrast, for ETW CB specimens, the failure mechanism observed at the fracture surface is a combination of two Modes: adhesive failure and light fibre tear failure. The colour changes in areas, from yellow to orange, where the adhesive predominates, indicating the onset of degradation caused by hygrothermal conditioning. According to Fernandes et al. [22], the yellowing of the resin indicates that degradation has occurred, and the material has aged. SEM analysis was later used to understand the delamination process of this type of degradation in joint technology.

The red lines show how far the crack has propagated during the fast

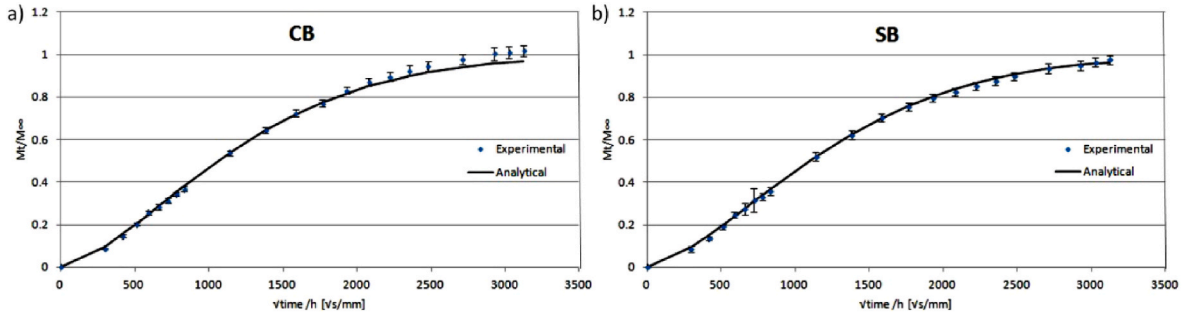

Fig. 2. Analytical and experimental data for moisture absorption of a) CB and b) SB specimens.

slip phase, which corresponds to the dark areas, while the slow and stable crack growth is related to the lighter grey stripes.

Stick-slip behaviour occurs due to local variations of the material systems [29,30], in this case attributed to the heterogeneous nature of the adhesive, which is composed of epoxy resin and a diamond-shaped polyester network. This adhesive has two functions: The first is to maintain homogeneous spacing between the laminates, and the second is to provide mechanical toughness by creating obstacles that slow the propagation of cracks in the joint region. Consequently, the crack growth behaviour changes from stable and continuous to unstable, altering the failure mechanism from cohesive to adhesive due to deviations in the crack tip path. Stick-slip behaviour can be explained by the formation of a plastic region at the crack tip soon after unstable growth. Propagation slows while the crack remains within this region as it tries to overcome the physical barrier in front of it. This is followed by rupture, where the crack quickly enters the 'unobstructed' region of material that had not been affected until then [31]. Hunt, Kratz and Partridge related stick-slip behaviour to the transition from cohesive to interlaminar failure modes. The Loctite® EA 9695 adhesive was positioned on a polyester web in its central plane to maintain a homogeneous thickness of 0.226 ± 0.3 mm throughout its length [32]. Other variations can influence this phenomenon, such as fibre-rich regions along the longitudinal direction, misalignment of fibres and voids, as well as fibre bridging or fibre bundles [20].

Fig. 4 shows a schematic of the path taken by the crack in the ETW CB Mode I test. This composite has five different layers: 1) the uncured laminate, 2) the interfacial plane, called interleaf region PS1; 3) the adhesive region; 4) the interfacial plane called interleaf region PS2, and 5) the cured laminate. The interleaf is a region where a tough material, a thermoplastic dispersed particle consisting of modified amorphous polyamide, is inserted between layers of composite material to enhance the thermosetting matrix damage tolerance. The interfacial plane PS2 was found between the adhesive and interleaf region (PS2a) and between the interleaf region and cured laminate (PS2b).

Fracture propagation was not observed in the PS1 plane; conversely, all the features manifested between the PS2a and PS2b planes (Fig. 2). The PS1 plane comprises the adhesive layer that is in contact with the uncured matrix resin layer. Both layers are cured simultaneously. The main reason for the absence of crack propagation is that adhesion by interdiffusion occurs at this interface during the mutual curing process of both layers. Interdiffusion occurs when macromolecules diffuse across the interface, creating an interphase and promoting adhesion strength between the contacting polymers (adhesive and substrate) [33]. This mechanism implies that the macromolecular chains or chain segments are sufficiently mobile and mutually soluble, and occur when the temperature is above the glass transition temperature, and the substrate and adhesive must be compatible [34]. This interphase is extremely strong and difficult to break due to the chemical bond that occurs between the polymer chains.

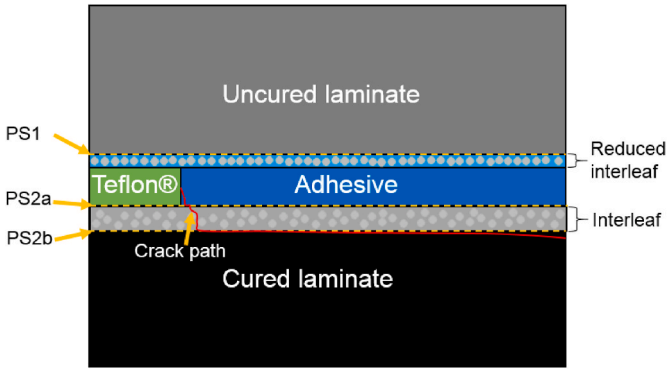

Fig. 4. Side view from CB joints and an indication of the interfacial planes and initial crack path: S1 specimen's side-cured Laminate, S2 specimen's side-uncured laminate.

In the PS2b plane (Fig. 4), the adhesion process called mechanical interlocking occurred. This process occurs when the irregularity of the surface of a substrate aids in the adhesion of the adhesive, and depending on the adhesive, it can penetrate the irregularities of the adhesive before it is completely cured. Pores, cavities and surface roughness contribute to mechanical interlocking. This occurred because the substrate S2 (Fig. 4) had already been previously cured before being in contact with the adhesive. Therefore, during the curing process of the composite joint, the adhesive filled the cavities of the laminate, without chemical bonds promoted by the curing process between the substrate and the adhesive occurring, only mechanical interlocking occurred, and the energy required to break this interface is lower when compared to the phenomenon of adhesion by interdiffusion.

The R curves for the RTA and ETW specimens are shown in Fig. 5a and 5b, respectively. At the beginning of the propagation process, the initial values of the G_{IC} to RTA specimens are higher than those of the ETW specimens, as observed in the dotted yellow circle. However, it is evident from these statistics that the ETW specimens have greater G_{IC} values than RTA specimens, as evidenced by the zone demarcated by the dotted green lines. Thus, when comparing RTA and ETW samples, although the G_{IC} value remains lower for ETW joints, it increases throughout the delamination process compared to the initial values. This is due to fibre bridging occurring in these specimens throughout the delamination process.

Fig. 6a shows the beginning of crack propagation on the S1 specimen's side, after the Teflon insert. In SEM figures, the crack propagation will always be considered from left to right as indicated by the arrow in Fig. 6. The adhesive surface was seen in the specimen extremity during the first fracture (Fig. 6a.A), and the failure Modes on the adhesive surface were seen when the image was magnified (Fig. 6b). Peel marks on the adhesive surface between the adhesive and the resin have a convex appearance. This can be seen as a curved or rounded surface aspect outward on one side of the sample, S1 side (Fig. 6b.A). This indicates that the S2 side was cured with peel-ply before. Typically, the purpose of the peel-ply fabric during the manufacturing process is twofold: first, to shield the laminate surface from damage during the curing process, and second, to promote a roughness on the laminate surface that enhances mechanical interlocking during the composite joint manufacturing process. Numerous fracture characteristics that happened throughout the delamination process on this specimen surface are shown in Fig. 6b.A. The smooth appearance of the peel-ply in Fig. 6b.A, explains the adhesive failure observed between the adhesive and the matrix contact. The lack of interdiffusion of the adhesive polymer chains at this interface, combined with the immobility of the polymer chains in the cured laminate matrix, as represented by the S2 surface, may have contributed to the adhesive failure. This is because the mobility of the polymer chains depends on the molecular packing or crosslinking that occurs when both resins are uncured [35].

Fig. 6b.B shows a cohesive failure on the resin as a result of the adhesive's rough appearance; Fig. 6b.C shows details of fibre imprint and insufficient fibre, which is characterised as a light-fibre tear failure; and Fig. 6b.D shows a smooth appearance, but also indicates an unstable delamination propagation region on the S1 specimen's side.

To better understand how the crack propagation moves from the adhesive plane to the first layer containing carbon fibre/matrix, as seen in Figs. 4 and 7 presents the magnification of this region on the S2 specimen's side. Fig. 7a and 7b shows a quick transition between failure modes. Three distinct aspects can be identified: i) Fig. 7b.A shows a cohesive failure in the adhesive due to its rough texture; ii) Fig. 7b.B shows a careful analysis of Fig. 7c, revealing an adhesive failure through the peel-ply marks, and iii) Fig. 7b.C shows a fibre imprint.

Fig. 7c shows peel-ply markings with cohesive and adhesive failure mechanisms, which is also seen from peel-ply markings, where the yellow arrow signifies the propagation of adhesive failure to the layer. The adhesive failure is seen in Fig. 7c.A and in Fig. 7c.A. The feather

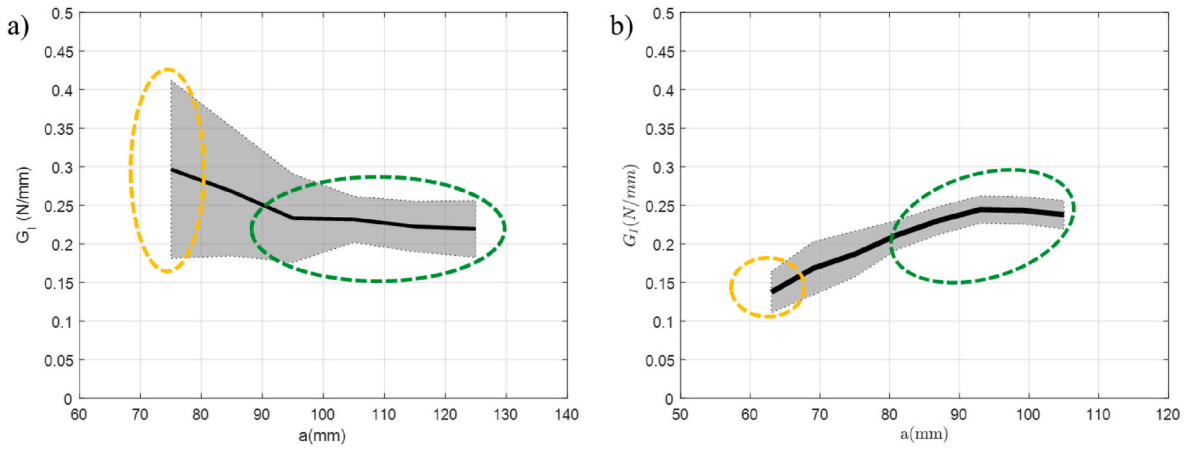

Fig. 5. CB fracture surface of a specimen tested under Mode I load. a) Mode I energy release rate in RTA, adapted from Brito et al. [2] and b) Mode I energy release rate in ETW conditioning.

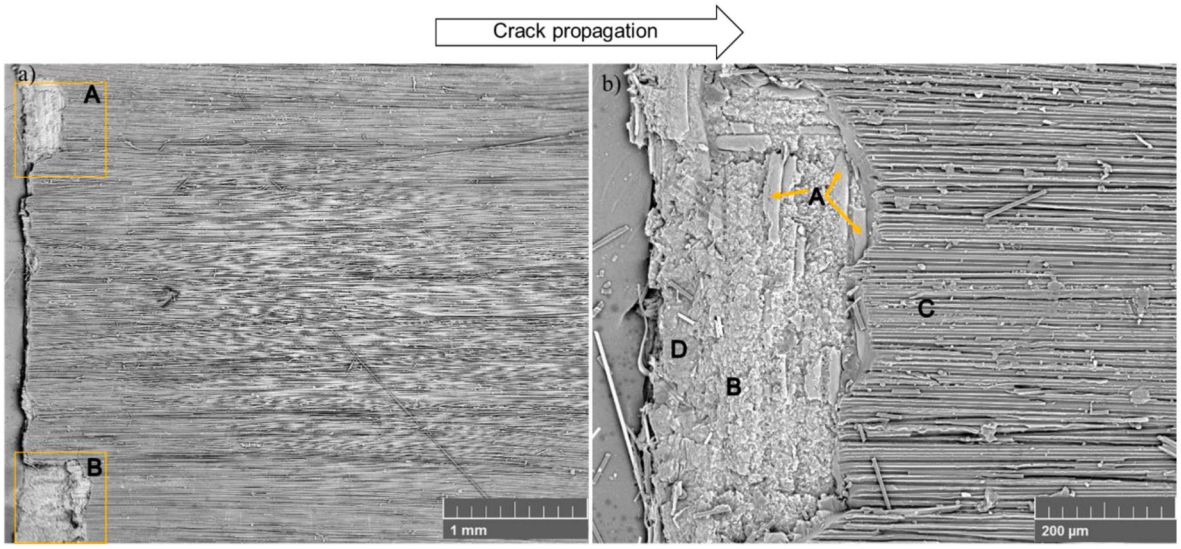

Fig. 6. CB fracture surface of the S1 specimen's side tested at the ETW conditions under Mode I load. a) Initial crack with detail "A", and in b) it is possible to observe peel-ply marks. Magnification of 51x and 250x, respectively.

aspect that travels from the fibre imprint to Fig. 7c.C is depicted in Fig. 7d.B. Particles, that exhibit the failure across the entire interleaf, are in Fig. 7c.C. Notably, the feather feature was always seen to appear as an orientation perpendicular to the fracture growth route, which started at the fibre or fibre imprint (Fig. 7d.B). These areas often have greater cross-link density volumes put into a matrix with comparatively lower cross-link densities. These nodules produce a granular texture and are oriented in clusters in the direction of fracture propagation. The well-known river marks are created where these crack fronts meet the tiny fracture plane perturbations required for convergence. These crack fronts may begin and progress on slightly different planes. The direction of local fracture propagation is evident from the feathering marks.

Fig. 8 shows three distinct characteristics that are evident at the beginning of the fracture on the S2 specimen's side, opposite region indicated in Fig. 6a.B and 7.a.B, representing the cured laminate. The first characteristic is represented by the rough texture of the adhesive and the presence of detached thermoplastic dispersed particles resulting from degradation (Fig. 8A). After exposure to water, the particle, previously linked to the polymeric structure in some manner, adopts a spherical shape and detaches from the matrix. The bonding between particles and resin in incompatible blends is sustained by van der Waals forces, which are relatively weak [36].

Disruption of this bond is not a challenge, as it may occur during interactions with moisture. The ability of the polyamide particle to absorb moisture from the ambient air is attributed to the hydrogen bonding facilitated by an oxygen atom within the polymer chain. An inherent trait of all polyamides, as indicated by Vlasveld et al. [37], is their capacity to absorb moisture from the environment. The second trait is exemplified by the presence of peel-ply marks (Fig. 8B), denoting adhesive failure in that region and exhibiting a smooth appearance in the cavities. The final characteristic is easily identifiable as a light-fibre-tear failure Mode, characterised by the presence of loosely dispersed fibres (Fig. 8C) and minimal resin content. It is also observed that crack-forming scarps are created from the convergence of two adjacent crack planes (Fig. 8D). The scarp is a particularly distinctive feature present in Mode I failure [33,38].

Fig. 9 further depicts the crack tip on the S2 side of the ETW CB specimen, which is represented by region C in Fig. 8. To further understand how the delamination process started, the failure aspects were cautiously observed. First, the crack moved from cohesive failure to the adhesive. Finally, it changed to the light fibre-tear failure Mode, presenting loose fibre from the fibre bridging process. The broken fibre caused by the fibre bridging is seen in Fig. 9a.A and its magnification in Fig. 9b. The fibre is often found in Mode I. During the Mode I process, the

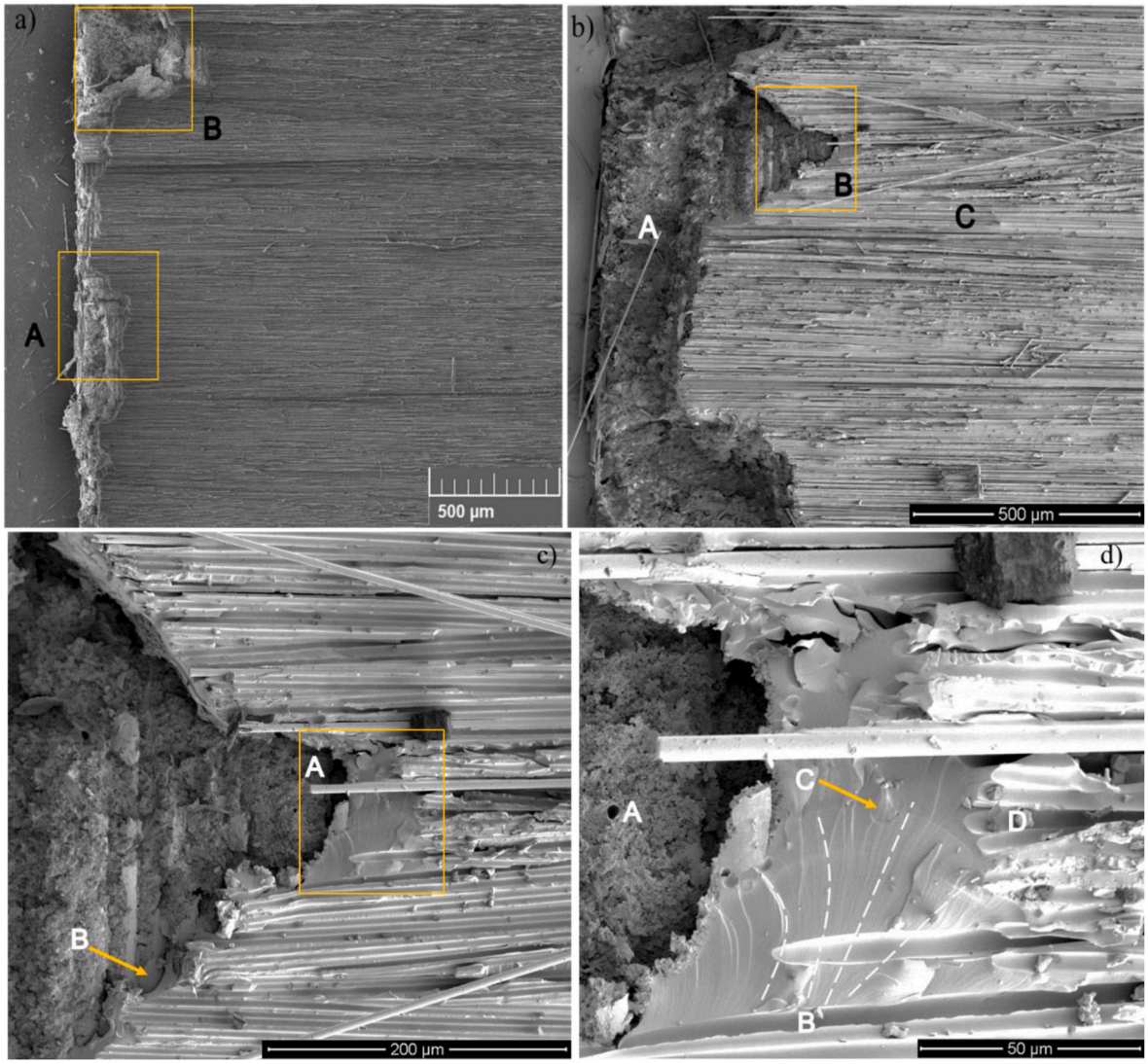

Fig. 7. CB fracture surface of the S2 specimen's side tested at the ETW condition under Mode I load. a) "A″ a detail of initial crack in bigger magnification in b), b) "A″ detail adhesive aspect, "B″ detail that has a magnification in c) and "C″ detail with fibre imprint, c)a transition of the planes with detail "A″ in magnification in d) and d) "A″ in adhesive roughness aspect, "B″ initial of feathering aspect, "C″ observed particles and "D″ fibre imprint. Magnification of 100x, 100x, 340x and 1000x, respectively.

fibre bridging results in a localised shearing of the matrix resin [39]. The fibre bridge causes the strength of the Mode I interlaminar fracture in composites to increase considerably because an interlacing of fibres is formed by causing the fibre to become degraded in the laminates on both sides of opposing faces, as is possible to observe in Fig. 4 [38,40]. Fig. 9a. B shows cusps in a resin-dominated area, indicating the occurrence of a Mode II failure process. Some characteristics may appear due to the formation of fibre bridging, which is not primarily Mode I characteristics, such as fibre fracture by tensile or the formation of small cusps. The cusps are caused in this case as fibres are being pulled from the surfaces during the crack opening, causing the material to exhibit a Mode II fracture aspect [38].

Fig. 10 shows a higher magnification of the initial failure of the S2 side of the ETW CB specimen. These fracture features can be found in transition regions between the cohesive fracture mode and the adhesive fracture mode, which are represented by areas B and C depicted in Fig. 6. As previously mentioned, the failure generally begins as a cohesive failure Mode in the adhesive. It becomes an adhesive failure Mode once it reaches the peel-ply region and propagates through the adhesive/resin interface until the particle deviates from the crack tip and the crack path reaches the fibre region. The "F" detail shows once more that the appearance of feathers happens perpendicular to the direction in which the crack propagates. This phenomenon may be caused by a high number of fibres near the start of the feathering aspect (Fig. 10F). Feathers are most likely present when a factor modifies the crack path locally.

Fig. 10E shows a crack that promotes the separation of the resin and changes the crack path from adhesive to laminate. Moreover, Purslow [41] described that frequently the fracture planes can be overlapped before they coalesce, producing a scarp on both surfaces and producing a ribbon, which may, Fig. 10b detail "C", remain attached to the fracture surfaces.

3.3. Failure aspects of ETW SB joints

A typical load versus displacement curve for SB ETW specimens is shown in Fig. 11. During the mechanical test, a stick-slip behaviour represents unstable (black areas) and steady (yellow areas) propagation, which means the combination of three failure Modes: fibre tear failure (black areas), light fibre tear failure (represented by a thin fibre layer on the adhesive surface) and adhesive failure (yellow areas without fibre), respectively. When compared to the RTA CB specimen [2], the same two

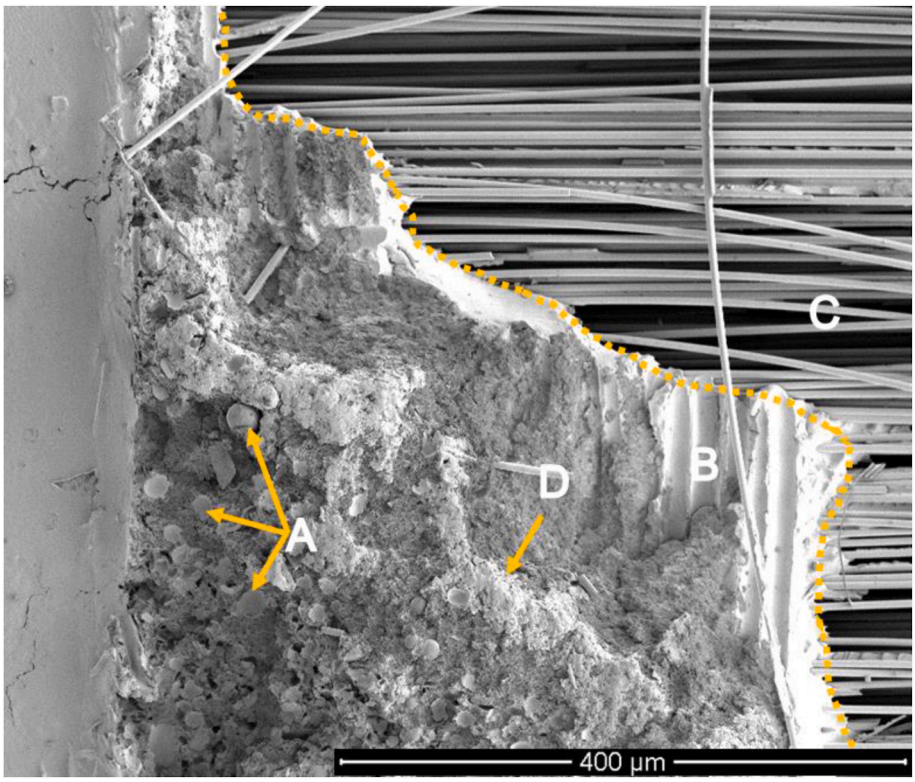

Fig. 8. CB fracture surface of a specimen tested at ETW condition under Mode I load. Features are evident at the beginning of the fracture on the S2 specimen's side (Fig. 7). The image represents the initial crack in an adhesive roughness area, "A" detail in detached particles, "B" detail in peel-ply marks, "C" detail in fibres and "D" scarps on the adhesive. Magnification of 200x.

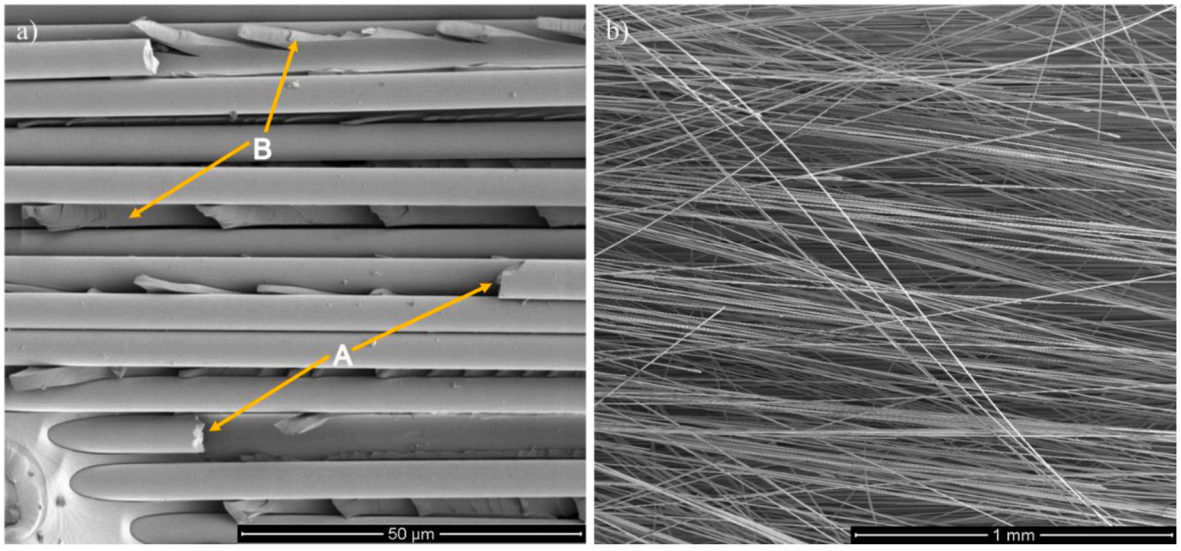

Fig. 9. CB fracture surface of the S2 specimen's side tested at ETW condition under Mode I load, magnification from Fig. 8C: a) "A" detail of broken fibres, "B" detail of cusps in a resin-dominated area with a magnification of 1500x and b) Loose fibres due to fibre bridging with a magnification of 500x.

failure Modes are observed in the fracture surface of the RTA SB specimen: the cohesive failure in the middle of the adhesive layer and the light fibre tear at the edge of the laminate, followed by a failure Mode dominated by fibre tear during delamination propagation [19].

Like the CB specimens at ETW conditioning, the SB specimen exhibits colour changes over the whole fracture surface of the specimen (Fig. 11). The colour of the specimen is noticed to be changing around the Teflon insert in comparison to other areas. This might indicate that the matrix's physical-chemical properties changed when exposed to increased moisture and temperature. ETW specimens had a G_{IC} value of 0.289 ± 0.098 N/mm, whereas RTA specimens had a value of 0.220 ± 0.068 N/mm, according to Brito et al. [2]. As a result, the G_{IC} in ETW conditioning was 31.36 % more than RTA.

To understand the crack propagation mentioned above, a side view of a fracture path from the SB specimen under Mode I load evaluated at the ETW condition is shown in Fig. 12. As observed in SEM analyses, it can be concluded that the crack can propagate along two paths: the interfacial planes between the interleaf and the cured laminate are

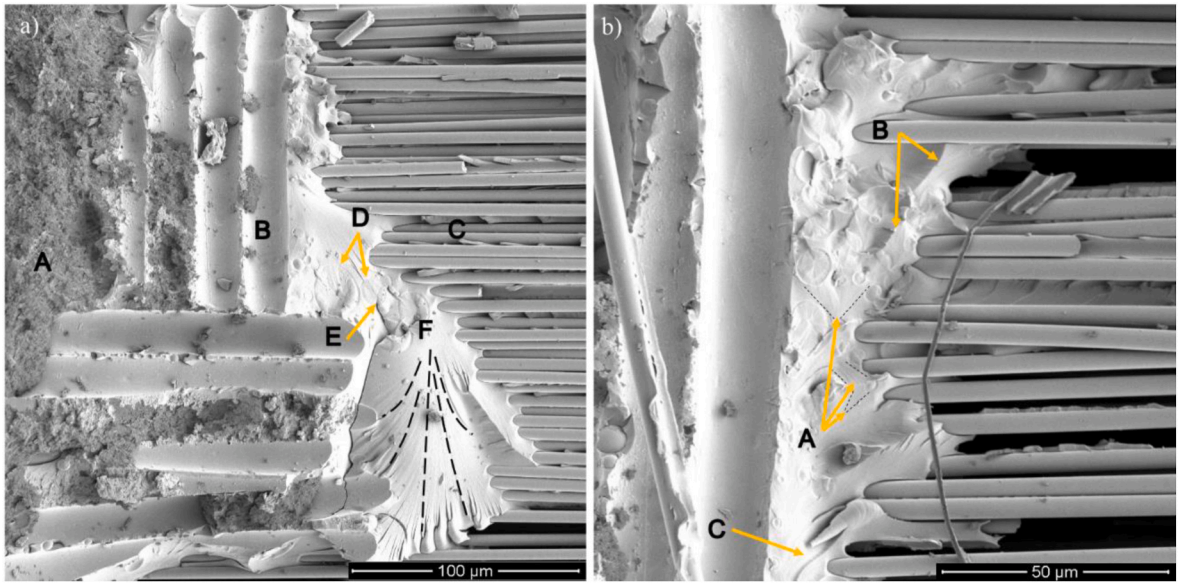

Fig. 10. CB fracture surface of the S2 specimen's side tested at ETW condition under Mode I load, magnification from Fig. 6 (transition regions B and C). a) A) Adhesive, B) Peel-ply imprint, C) Fibres, D) Particles, E) Initial crack, and F) Feathering aspect with a magnification of 500x and b) A) Texturized microflow and B) Scarp on resin and C) Scarp producing a ribbon with a magnification of 1000x.

designated as PS1a and PS2b, and the corresponding planes to the interfacial region between the adhesive and the interleaf are designated as PS1b and PS2a.

The R curves for the ETW and RTA specimens are shown in Fig. 13b and 13a, respectively. It is evident from these statistics that ETW specimens have greater propagation values than RTA specimens, as evidenced by the zone demarcated by the dotted green lines. However, when comparing RTA from Brito et al. [2] to ETW specimens, the hardness initiation values are greater for the former. The fibre bridging that happened on both sides of the specimens mostly explains this. Using SEM, the fracture aspects that occurred on the surface of this specimen were explored.

The S1 specimen's side from Fig. 11 will be examined first to determine the various failure aspects present in the specimen. Numerous SB specimens exhibit the same traits as those depicted in Fig. 14, where a catastrophic failure on the composite joint is evident by the adhesive layer debonding (Fig. 14a) from both planes PS1b and PS2a (as shown in Fig. 12). This catastrophic failure promoted a significant number of loose fibres (Fig. 14b) and obvious adhesive debonding (Fig. 14c) from the laminate. This behaviour was not related to Brito's work [2] nor Silveira's work [19] on RTA SB specimens. It clarified why and how this occurrence enhanced the material's fracture toughness throughout the spread of delamination, as determined through fractographic investigation.

Fig. 15 presents the adhesive layer on the S1 specimen's side that is loose, as was observed in Fig. 14. Fig. 15a.A, 15.a.B and 15.a.C identify the adhesive, interleaf, and fibre imprint, respectively. Fig. 15a.B shows the interlayer where the thermoplastic particles are located, and the magnification of this region can be seen in Fig. 15b.A, providing a better view of the details of the particles. There is evidence of particle debonding around it, which is consistent with the behaviour seen in ETW CB joints and can be caused by relaxation and plasticization. It was found that the initial fracture propagation in SB joints tested under RTA conditions happened in the centre of the adhesive layer [3,4,19]. On one side of the ETW specimen, however, the whole adhesive layer is visible. The deterioration that took place in this area led to ETW specimens having lower G_{IC} values compared to RTA specimens, as indicated by the yellow dotted circle in Fig. 13.

It is easy to see the adhesive in area C, the details of which are displayed in Fig. 16a and 16b, respectively, by looking at the S1 side of Fig. 12. The fibre imprint is seen behind the adhesive position. This is conceivable because the resin coating is so thin in this region that the adhesive between the fibre impression may be seen. This fracture feature will cause some significant considerations. One may see that Fig. 16 shows regions of distinct hue (whitish) in those parts where the adhesive is obvious, while simple fibres and resin are apparent in other areas. At times, the crack propagation travels near the adhesive layer and far from it.

This information raised the idea that the cracks spread for a different reason. After the specimen was analysed, it was found that the adhesive layer in the SB-conditioned specimen had debonded on both sides. In this instance, the SB joints had a mechanical interlock rather than a chemical bond since both sides had already undergone curing, which deviates from the adhesion hypothesis used for the CB specimen. As previously mentioned, the interdiffusion process could not occur between the adhesive's polymer chain and the laminate's polymer matrix due to the laminate's pre-curing process on the S2 side.

Hence, the mechanical interlock is significant in establishing the connection between the resin and adhesive layers. Depending on the adhesive, mechanical interlocking allows the irregularities on a substrate's surface to aid in adherence. The adherent's irregularities can be penetrated before hardening. Mechanical interlocking is facilitated by surface asperities, cavities, and pores. Certain surface treatments, like plasma treatment, leave noticeable pits that are easily filled by the epoxy resin with careful soaking. Adhesion can be improved by surface roughness, which can enhance the energy dissipated viscoelastically or plastically around the fracture tip and in the bulk of the material during joint failure, rather than necessarily coming from a mechanical mechanism [42,43].

Consequently, in the SB joints, the adhesive layer of the specimen detached from both surfaces, as shown in Fig. 14. Despite this, fibre bridges are present on both sides of the adhesive, indicating adhesive failure between the adhesive and the laminate. Ultimately, it was determined that the fibre bridge mechanism in this sample alters fracture propagation and increases the G_{IC}.

Fig. 17 brings details about both specimens' sides: S1 side (Fig. 17a) and S2 side (Fig. 17b). It is crucial to highlight that this specimen was previously cured with peel-ply on both sides, as shown by the concave and convex peel-ply imprints on both specimens' sides. For instance, in Fig. 17a.B, an adhesive failure is shown in the peel-ply imprint. Based on

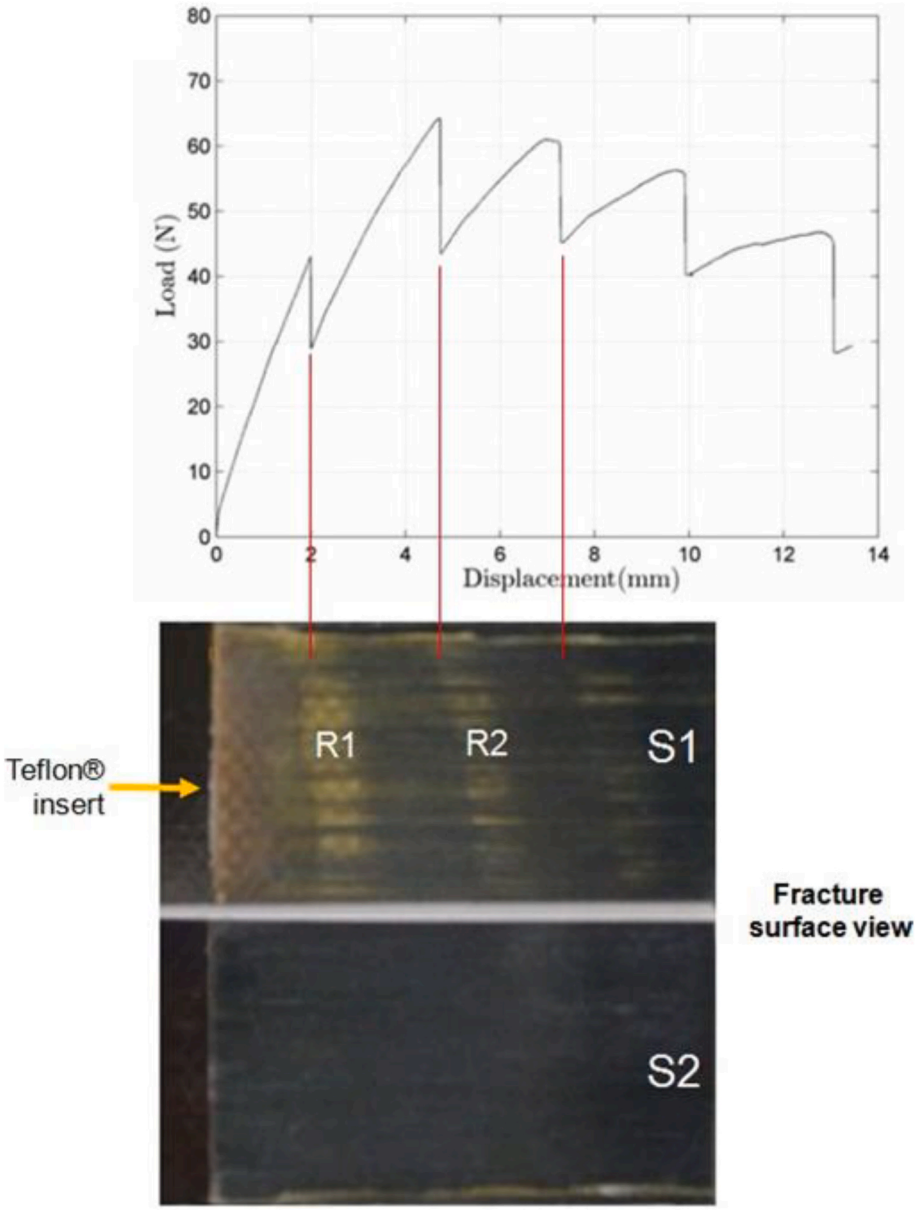

Fig. 11. Load versus displacement curve of SB specimen related to the pattern observed in its fracture surface in the ETW condition under Mode I load.

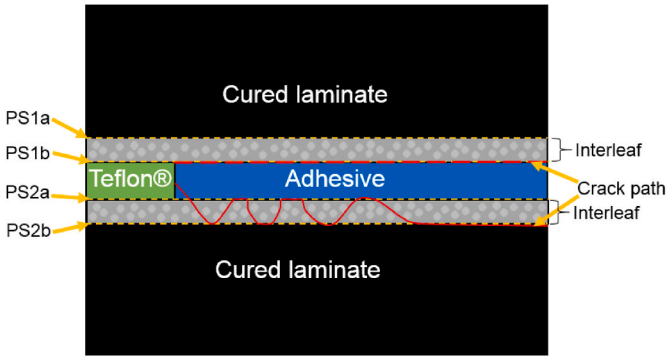

Fig. 12. Side view from the SB joints and an indication of the interfacial planes and initial crack path.

the convex peel-ply fabric form, it is understood that this shape originates from the specimen's S1 side.

This occurs because of the complete breakdown between the S2 side laminate and the adhesive. An alternative peel-ply fabric structure, with a concave shape (Fig. 17b.B), is shown from the S2 specimen's side. The smooth surface of the material suggests that adhesive failure has occurred in this locality. Similar behaviour was observed in Fig. 17a and 17b. The delamination process changes from an adhesive failure to a cohesive failure (Fig. 17b.A). When it reaches the region of adhesive failure, the failure plane changes again to an interleaf (Fig. 17b.C), a surface with several particles, and it continues to propagate for another layer (Fig. 17b.D), where fibre imprint can be seen. Thereby, it is classified as a light-fibre-tear failure according to ASTM 5573 [19]. Fig. 17a. B and 17.b B present a magnification of the adhesive-resin transition region.

A cohesive breakdown in the adhesive is seen in Fig. 18a.A, portion of the peel-ply indicates the location of the adhesive failure, on the S2 side of the specimen's surface. Particles (Fig. 18a.C) and feathering features (Fig. 18a.B) represent a failed transition into interleaf and are

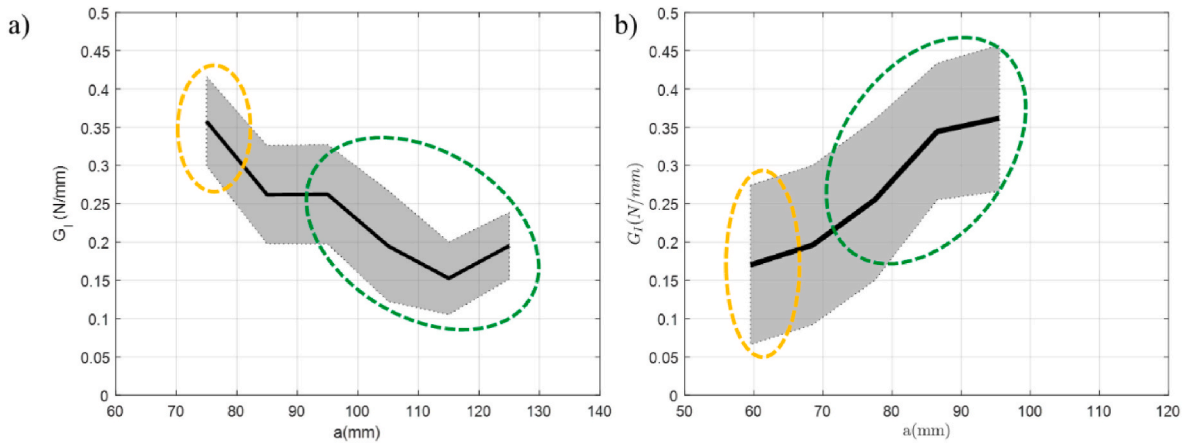

Fig. 13. SB joint fracture surface of a specimen tested at ETW condition under Mode I load. a) Mode I energy release rate in RTA, adapted from Brito et al. [2] and b) Mode I energy release rate in ETW conditioned specimen.

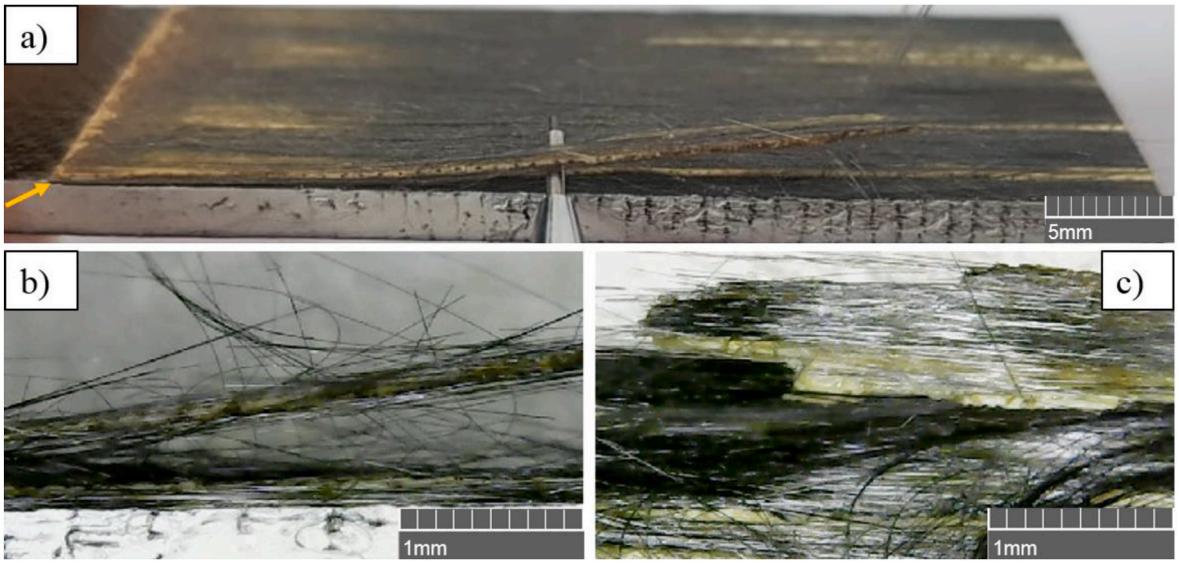

Fig. 14. SB joint fracture surface of the S1 specimen's side tested at ETW condition under Mode I load. a) Lateral image of the specimen. b) Fibre bridging and c) Adhesive failure.

detected close to this site. Once more, the feather aspect starts in a fibre imprint and changes the direction of the crack route locally. It is perpendicular to the direction in which the fracture propagates.

Lastly, fibre imprint in Fig. 18a.D is noticed. With a higher magnification, as seen in Fig. 18b. There is a coherent failure shown. Certain particle features (Fig. 18b.C) resemble the cusp seen in Fig. 18b.B, suggesting a cohesive failure occurred between the fibre and the resin. A microflow aspect into fibre impressions is present in Fig. 18b.D suggests the propagation from this region to the adhesive region presented in Fig. 18b.A.

The crack propagation transition from the adhesive layer to the fibre layer that occurred on the S2 specimen's side surface may be identified in Fig. 19. On the other hand, the polyester net node (Fig. 19a.B) and the crack path are shown altering the local area where the failure Mode has changed, creating a scarp on the adhesive surface (Fig. 19a.C). This phenomenon has already been seen in Brito's work [2], where the failure direction switches at the polyester net node. To understand how crack propagation moves into the fibre layer, a magnification of the region A shown in Fig. 19a is presented in Fig. 19b. In this Figure, several failure aspects are shown as the crack propagates from the adhesive layer to the resin layer and fibre layer. On the resin layer, a scarp can be observed, formed from two cracks from the front and some broken particles (Fig. 19b.A and 19.b B). In the region near the fibres, it is possible to observe some texturized microflow, feather aspects and cusps (Fig. 19b.C, 19.b.D and 19.b E).

3.4. SB and CB joint failure comparison subjected to ETW conditioning

Following the detailed fracture analysis of CB and SB specimens subjected to ETW conditioning, a metric was defined to quantify the frequency and magnitude of each failure identified on the specimens' surfaces to provide a comprehensive overview of the potential failures that may occur in these materials when exposed to Mode I load and environmental factors. The aspects have been divided into mechanical interlocking and chemical bonding processes, in addition to the failure aspect studies. To be more realistic, the works of Silveira [19] and Brito [2,3] were analysed, and the failure aspects observed in the surface of the RTA CB and SB specimens were considered for comparison with the results presented here in Table 1.

Table 1 corresponds to all Mode I failures found and is ranked according to the intensity with which they were observed. The intensity of appearance of the failures following notations: One black circle: low-

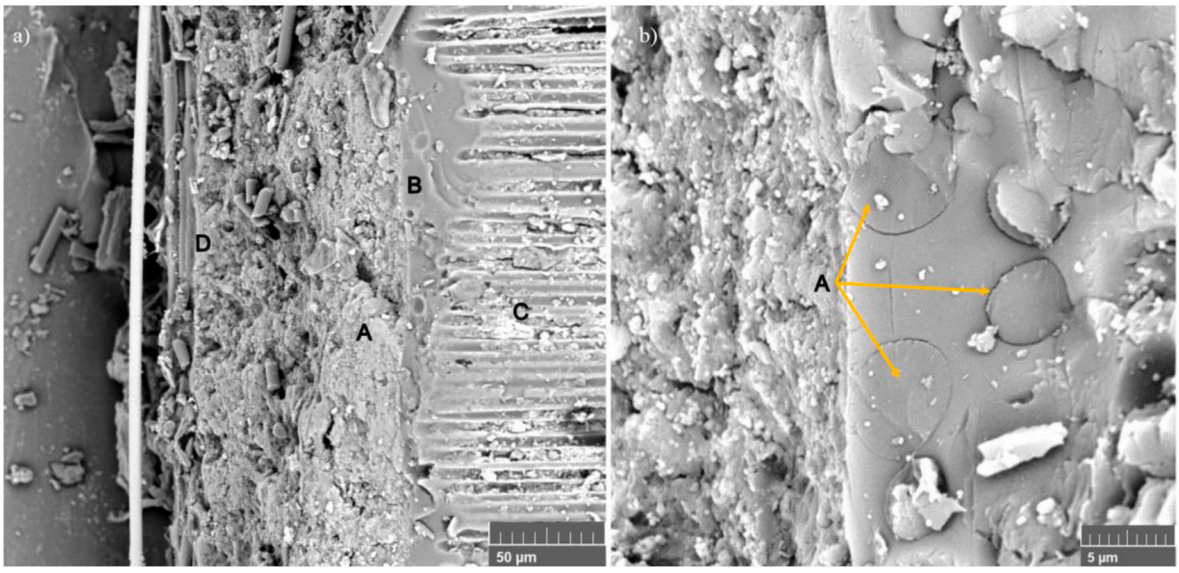

Fig. 15. SB joint fracture surface of the S1 specimen's side tested at the ETW condition under Mode I load. a) Initial crack after Teflon insert with "A" detail of adhesive layer, "B" detail of interleaf, "C" detail of fibre imprint, and "D" debris, and b) "A" detail of particle in the initial crack. Magnification of 800x and 7000x, respectively.

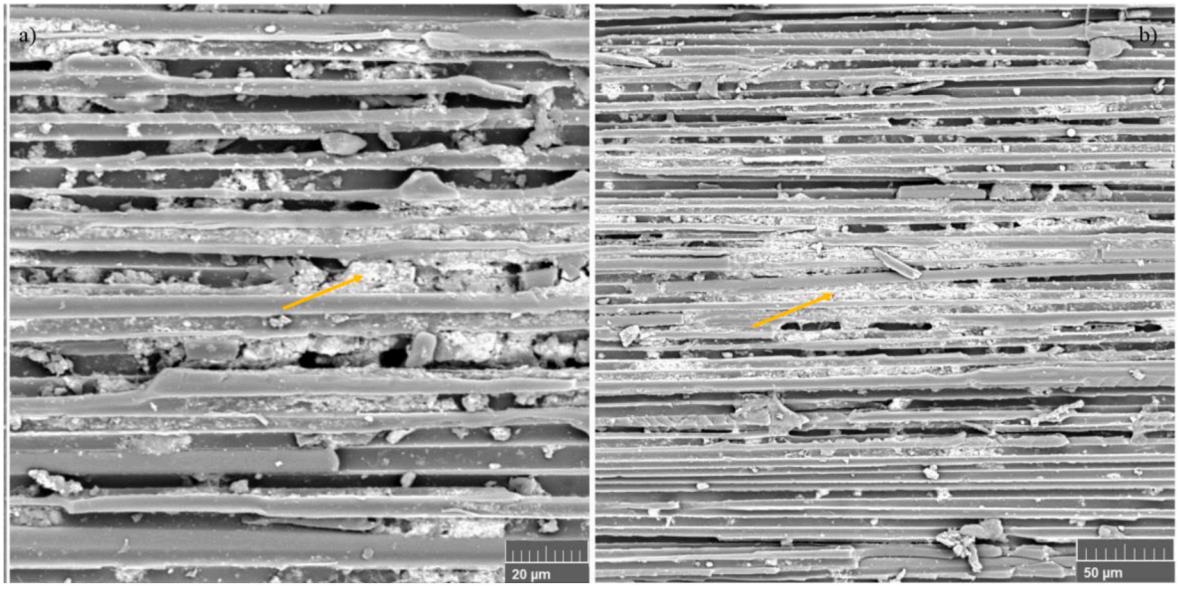

Fig. 16. SB joint fracture surface of S1 specimen's side tested at ETW condition under Mode I load, represented by Fig. 16C. Magnification of a) 1500x and b) 700x, respectively.

intensity; Two black circles: medium intensity; Three black circles: high-intensity; Empty circle: the failure aspect not observed; Trace: aspect does not correspond to the joint, failure Mode or loading, *: for occurrences only near the Teflon insert, and **: for more pronounced occurrences near the Teflon insert, but also observed with less intensity in the rest of the specimen.

The CB and SB joints evaluated in Mode I at RTA and ETW conditioning are compared in Fig. 20. The graph was made using the data from Table 1. The X-axis shows the abbreviations for the failure features, and the Y-axis shows the frequency of each failure.

Fig. 20 presents the failure aspects of CB and SB specimens under Mode I at RTA and ETW conditioning.

Fig. 20a, it observed mainly seventeen and sixteen failure aspects of CB joints under Mode I when comparing RTA and ETW conditioning, respectively, where the smooth appearance of the adhesive, fibre bridging, and fibre imprint was the most relevant in RTA [2,3,19]. The manufacturing process used to obtain the CB joint caused the uncured side of the chemical laminate to chemically bond to the adhesive, promoting a chemical bonding mechanism and thus increasing the mechanical strength of the "uncured" interface with the adhesive. Therefore, the initial crack will propagate preferentially in the region of lowest mechanical strength, i.e. in the adhesive, promoting cohesive failure of the adhesive and thus giving rise to the appearance of the failure aspect called roughness on the surface of the adhesive.

Fig. 20b, it was observed that mainly sixteen and twenty-one failure aspects of SB specimens under Mode I in RTA and ETW conditioning, respectively, where the failure occurred by the polyester net node, broken fibres, fibre bridging, roughness and smooth appearance on the adhesive were the most relevant in RTA.

Due to the manufacturing process and its interlocking mechanism,

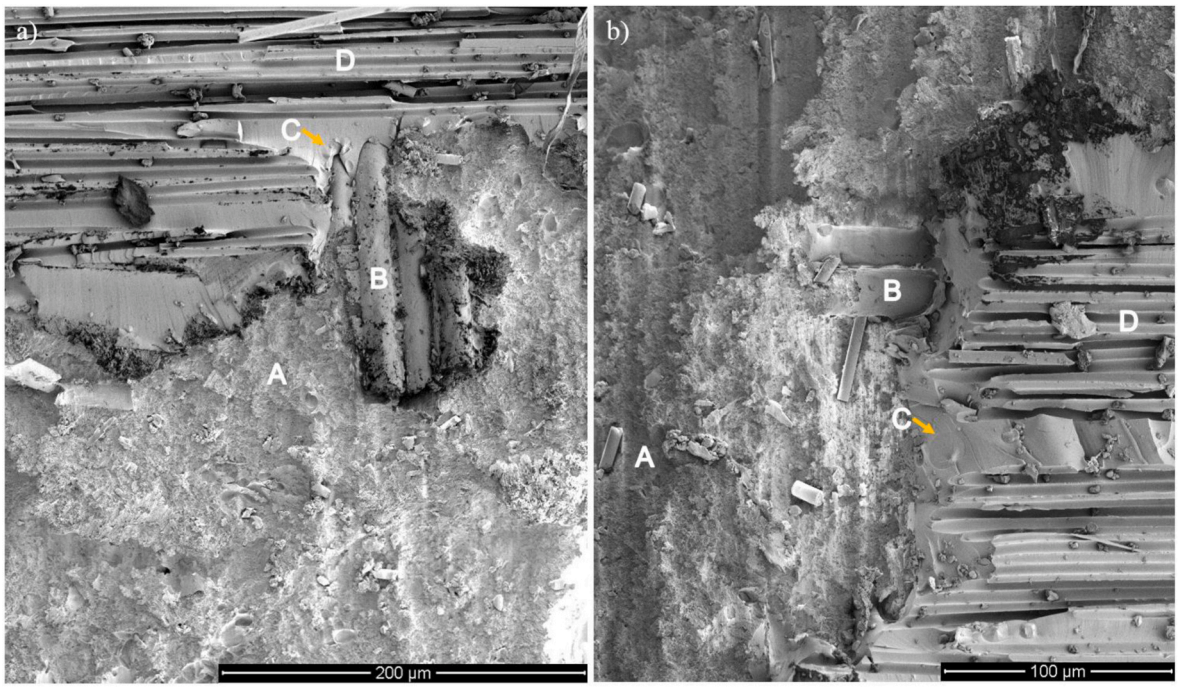

Fig. 17. SB joint fracture surface of a specimen tested at ETW condition under Mode I load. a) Initial crack in the S1 specimen's side and b) S2 specimen's side. Magnification of 400x and 500x, respectively.

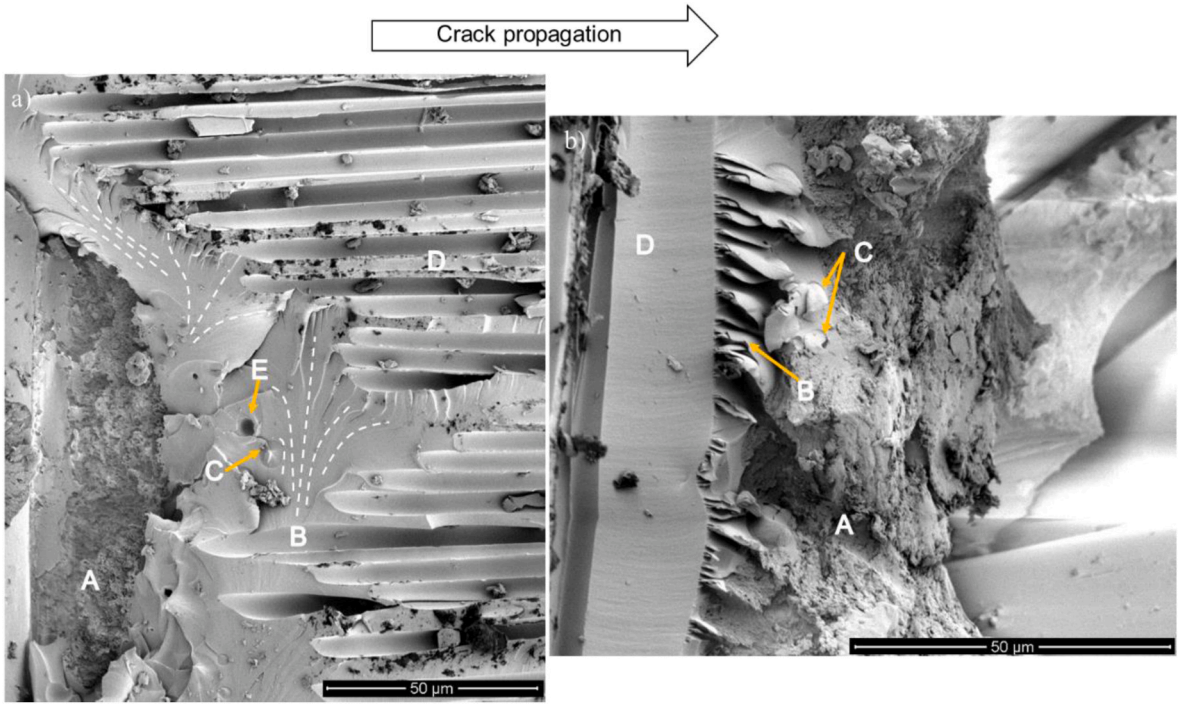

Fig. 18. SB joint fracture surface of the S2 specimen's side tested at the ETW condition under Mode I load. Images a) 1000x and b) 1500x present a magnification of the initial failure close to the Teflon insert.

the SB specimens had a greater number of failure aspects. It was observed that seventeen and twenty-one failure aspects were observed in CB and SB, respectively. Fibre bridging, fibre imprints and broken fibres were the most relevant failure aspects that occurred in these specimens. In SB specimens, the light-fibre-tear failure occurred on both sides of the adhesive; because of this, the fibre bridging intensity was considered greater than in the CB specimen. Also, in SB specimens, the fibre imprint was greater than in CB specimens because of the type of interlocking mechanism. Therefore, the G_{IC} was higher in SB specimens at ETW conditioning than in CB specimens due to the fibre bridging that occurred on both sides of the adhesive. However, it is important to emphasize that the failure occurred in two planes, which is worse for bonded joints.

The second most significant aspect of both ETW specimens is the

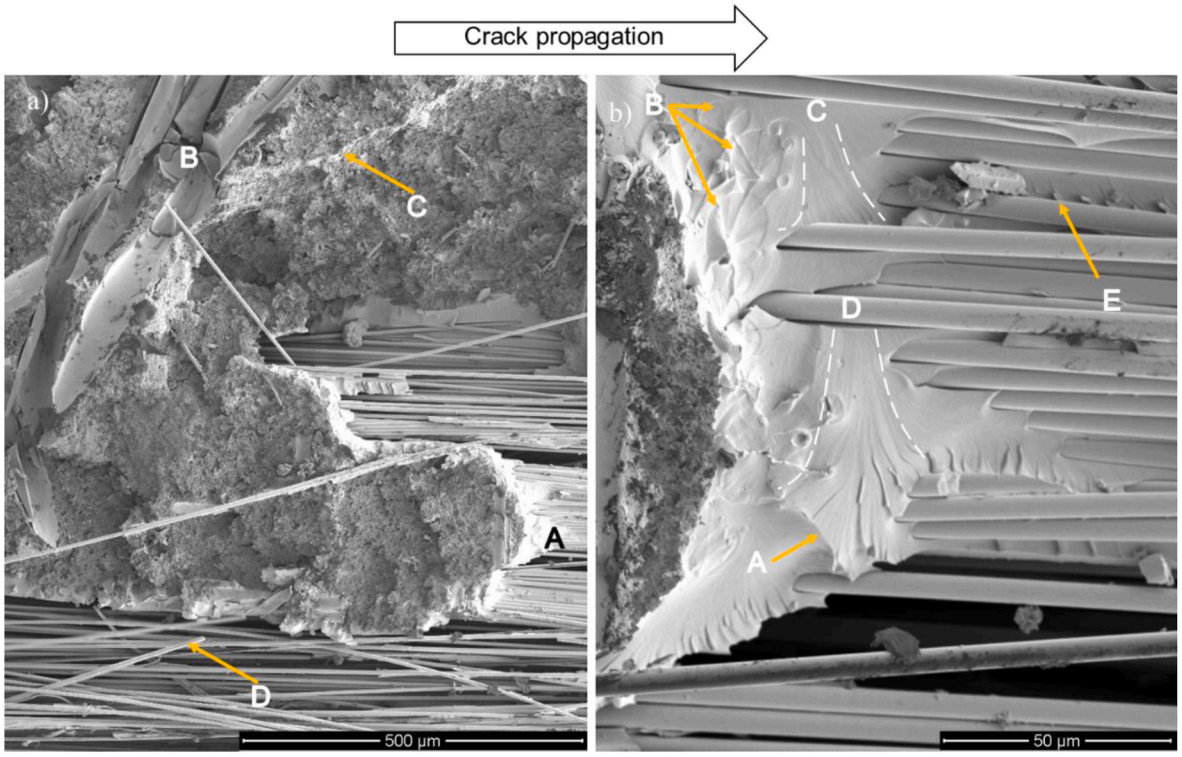

Fig. 19. SB joint fracture surface of the S2 specimen's side tested at the ETW condition under Mode I load. The transition of failure from adhesive to fibre layer. a) A) Transition of crack path, B) Polyester net node imprint, C) Scarp on the adhesive, and D) Broken fibre with a magnification of 150x and b) A) Scarp on resin, B) Texturized microflow, C) Cusps on matrix and D) Feather aspect. Magnification of 1000x.

Table 1
Failure aspects in Mode I correlated with SEM images.

NO	FAILURE ASPECT	Abv	CB		SB	
			RTA	ETW	RTA	ETW
1	Broke fibres	BRF	●	●●	●●	●●
2	Cleavage by fibre bridging	CFB	○	○	○	●●●
3	Cusps (fibre region)	CFR	●	●	●	○
4	Cusps (matrix region)	CMR	○	●	○	●
5	Debris	DBR	○	○	○	●●●
6	Failure in two planes	FTP	–	–	○	●●●
7	Failure occurred by Polyester net node	FPN	●	○	●●●	●
8	Feather	FTH	●	●	●	●●
9	Fibre bridging	FIB	●●	●●●	●●	●●●
10	Fibre imprint	FII	●●	●●●	●●	●●●
11	Loose particle	LPT	–	●●*	–	●●*
12	Microcracks	MCR	○	●*	●	●
13	Particle deformed	PDF	●	●	●	●
14	Particle pullout	PPO	●	○	●	●
15	Peel ply (Adhesive failure)	PPA	●	●●*	●	●●
16	Peel ply (Cohesive failure)	PPC	●	●*	●	●
17	Resin deformation (plasticization)	RDF	–	●●	–	○
18	Ribbon	RBB	●	○	○	○
19	River lines	RIL	●●	○	●	●●
20	Roughness appearance on the adhesive	RAA	●	●●*	●●	●
21	Scarp on the adhesive	SAD	●●	●*	●●	●
22	Scarp on the resin	SRS	●	●*	●	●
23	Smooth appearance on the adhesive	SAA	●●●	●*	●●	●*
24	Texturized microflow	TMF	●	●	○	●

loose particles and peel ply aspects attributed to the adhesive failure. The loose particles are the factor that decreases the value of fracture toughness at the beginning of both specimens, as can be seen in Fig. 5b and Fig. 13b.

Low-intensity aspects, such as textured microflow and scarps on the resin surface and the adhesive surface, are common to both joints as they are failure aspects caused by crack progression during the delamination process.

4. Conclusions

A comparative analysis was conducted to comprehend the failure mechanisms of composite joints under different environmental conditions.

In the case of CB joints conditioned with ETW, a colour difference was observed in the conditioned joints and a reduction in fracture toughness compared to SB specimens. The failure occurred on the side of the specimen that was previously hardened. However, the G_{IC} values were lower near the Teflon insert and increased throughout the specimen. This is due to the adhesive degradation and particulate material at the beginning of the specimen, and the fact that the adhesive failures in the peel-ply impressions were followed by a fibre-bridging process, a phenomenon that increases the fracture toughness of the material.

SB joints in ETW conditioning showed an unexpected fracture toughness value (G_{IC}) that increased with hygrothermal conditioning. However, during analysis, the reason for this increase was understood. As with CB joints in ETW conditioning, the crack in SB joints went through the adhesive and the previously cured laminate. However, as both sides were previously cured in the SB joints, the crack went through both sides, significantly increasing the fracture toughness values. The high toughness of one side of the material due to fibre bridging caused the layer on the other side to be exposed to the adhesive, resulting in fibre bridging on both sides of the adhesive layer. In addition, the side that became accessible to the SEM technique after the mechanical test showed between the fibre imprints of the adhesive material in some places, indicating that the crack went through a sinuous path as once the fibre bridging changed the crack to the laminate from one side of the adhesive and after to the other side of the adhesive, causing a lot of energy to be fractured.

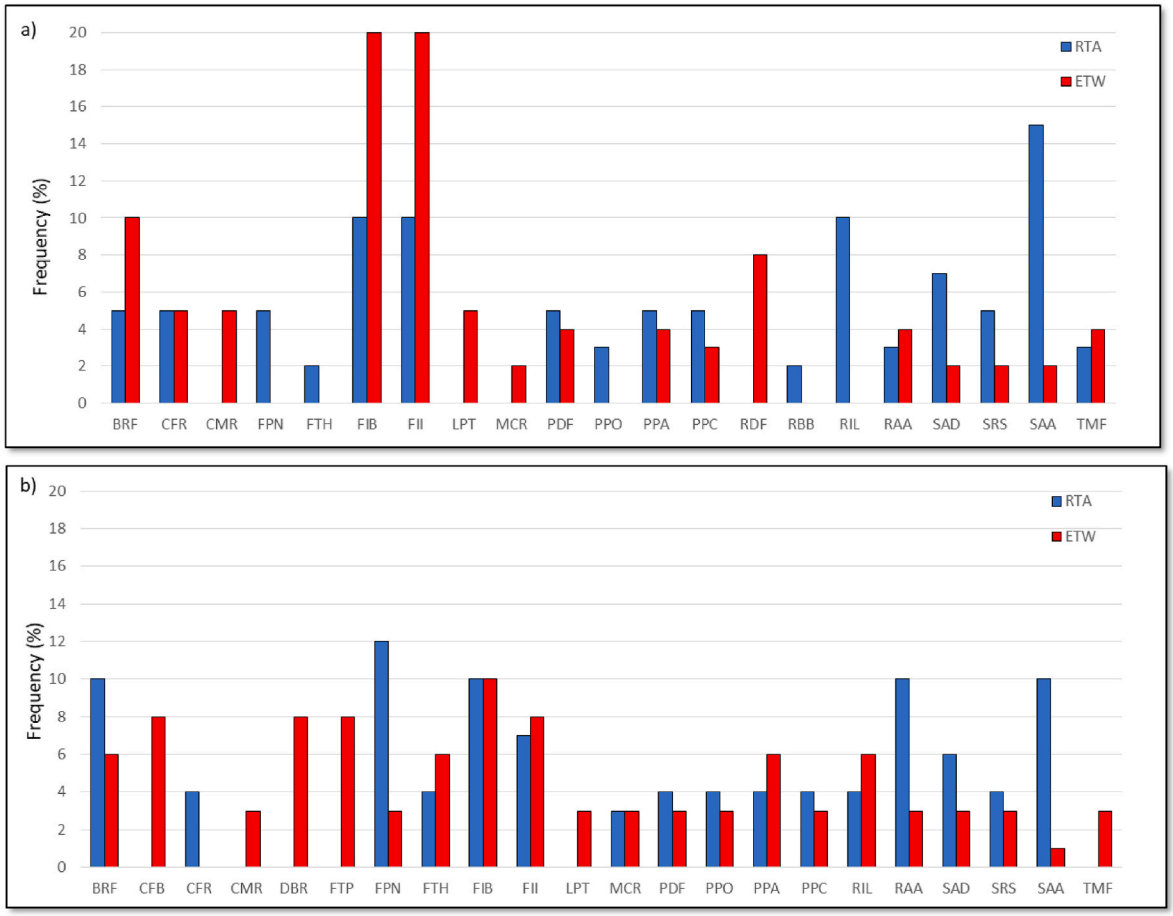

Fig. 20. Comparison of failure aspects of a) CB joints and b) SB joints under Mode I.

Using the fractography technique, it was possible to identify and compare the failure aspects and conclude that, although the SB specimens had a higher G_{IC} than the CB specimens, the SB joint degradation process was more intense when subjected to ETW conditioning.

CRediT authorship contribution statement

Núbia N.A. Silveira: Methodology, Investigation, Writing – original draft, Formal analysis. **Camila B.G. Brito:** Writing – review & editing, Formal analysis, Methodology. **Geraldo M. Cândido:** Visualization, Investigation. **Maurício V. Donadon:** Visualization, Project administration, Resources, Funding acquisition, Supervision, Conceptualization. **Rita C.M. Sales-Contini:** Writing – review & editing, Supervision, Writing – original draft, Formal analysis, Methodology.

Declaration of competing interest

The authors declare that they have no known competing financial interests or personal relationships that could have appeared to influence the work reported in this paper.

Acknowledgements

This project is partially supported by the CNPq processes 126346/2016-0, 142761/2016-8, 800319/2016-8 and 800392/2016-7, CAPES 1643501, CAPES/ITA (Process 88887.142318/2017–00), FINEP 0114018300 and FAPESP 2015/16733-2. The authors also acknowledge the Laboratory of New Concepts in Aeronautics and the Laboratory of Materials and Processes at ITA for providing the infrastructure and equipment needed for the development of this work.

Data availability

No data was used for the research described in the article.

References

[1] Budhe S, Banea M, Barros S De, Silva L da. An updated review of adhesively bonded joints in composite materials. Int J Adhesion Adhes 2017;72:30–42. https://doi.org/10.1016/j.ijadhadh.2016.10.010. 2017.
[2] Brito CBG, Contini RCMS, Gouvêa RF, Oliveira AS, Arbelo MA, Donadon MV. Mode I interlaminar fracture toughness analysis of Co-bonded and secondary bonded carbon fibre reinforced composites joints. Mat Res 2017;20:873–82. https://doi.org/10.1590/1980-5373-MR-2016-0805.
[3] Brito CBG, Sales RCM, Donadon MV. Effects of temperature and moisture on the fracture behaviour of composite adhesive joints. Int J of Adhes and Adhesiv 2020;100:102607. https://doi.org/10.1016/j.ijadhadh.2020.102607.
[4] Shiino M, Francis González, Ramírez M, Parise Garpelli F, Alves Da Silveira N, Mendonça Sales RDC, Donadon MV. Interlaminar crack onset in co-cured and co-bonded composite joints under Mode I cyclic loading. Fatig and Fract of Eng Mat and Struc 2019;42(3):752–63. https://doi.org/10.1111/ffe.12949.
[5] Mamalis D, Floreani C, Brádaigh M. Influence of hygrothermal ageing on the mechanical properties of unidirectional carbon fibre reinforced powder epoxy composites. Comp Part B Eng 2021;225:109281. https://doi.org/10.1016/j.compositesb.2021.109281.
[6] Park Y-B, Song M-G, Kim J-J, Kweon J-H, Choi J-H. Strength of carbon/epoxy composite single-lap bonded joints in various environmental conditions. Comp Struc 2010;92(9):2173–80. https://doi.org/10.1016/j.compstruct.2009.09.009.
[7] Tracy J, Yin Y, Yang J, Osborne JC, Blohowiak KY, Dauskardt R. Environmentally assisted crack growth in adhesively bonded composite joints. Comp Part A Appl Sci and Manuf 2017;102:368–77. https://doi.org/10.1016/j.compositesa.2017.08.018.
[8] Sales RCM, Sousa AF de, Brito CBG, Sena JLS, Silveira NNA, Cândido GM, Donadon MV. Analysis of hygrothermal effects on mixed Mode I/II interlaminar fracture toughness of carbon composites joints. Int J Adhesion Adhes 2020;97:102477. 1016/j.ijadhadh.2019.102477.
[9] Xu D, Liu P, Li J, Chen Z. Damage Mode identification of adhesive composite joints under hygrothermal environment using acoustic emission and machine learning.

Comp Struct 2019;211:351–63. https://doi.org/10.1016/j.compstruct.2018.12.051.
[10] Shishesaz M, Hosseini M. Effects of joint geometry and material on stress distribution, strength and failure of bonded composite joints: an overview. J Adhes 2018;96(12):1053–121. https://doi.org/10.1080/00218464.2018.1554483.
[11] Budhe S, Banea M, Barros S. Bonded repair of composite structures in aerospace application: a review on environmental issues. Appl Adhes Sci 2018;6:3. https://doi.org/10.1186/s40563-018-0104-5.
[12] Abdel-Monsef S, Abdel-Monsef S, Renart J, Carreras L, Turon A, Maimí P. Effect of environment conditioning on Mode II fracture behaviour of adhesively bonded joints. Theor Appl Fract Mech 2021;112:102912. https://doi.org/10.1016/J.TAFMEC.2021.102912.
[13] Olander R, Tracey A, Grace W, Flinn B. Nanoscale property characterization of composite adhesive bonding systems with long-term environmental exposures. Proceedings of the ASME 2024 aerospace structures, structural Dynamics, and materials Conference. ASME 2024 aerospace structures, structural Dynamics, and materials Conference. ASME; April 29–May 1, 2024. https://doi.org/10.1115/SSDM2024-121492. Renton, Washington, USA, V001T03A019.
[14] Silveira NN, Sales RC, Cândido GM, Donadon MV. Fractographic analysis of the hygrothermal effect in co-bonded and secondary bonded joints under Mode II delamination loading. Int J Adhesion Adhes 2020;98:102508. https://doi.org/10.1016/j.ijadhadh.2019.102508.
[15] 3900 prepreg system data sheet. Toray®. https://www.toraycma.com/wp-content/uploads/3900-Prepreg-System.pdf. [Accessed 30 April 2025].
[16] ASTM. D5528: standard test method for Mode I interlaminar fracture toughness of unidirectional fibre-reinforced polymer matrix composites. West Conshohocken, PA: American Society for Testing and Materials; 2013.
[17] Astm D5229/D5229M: standard test method for moisture absorption properties and Equilibrium conditioning of polymer matrix composite materials. West Conshohocken, PA: American Society for Testing and Materials; 2012.
[18] Wang Q, Chen T, Wang X, Zheng Y, Zheng J, Song G, Liu S. Recent progress on moisture absorption aging of plant fibre reinforced polymer composites. Polymer 2023;15(20):4121. https://doi.org/10.3390/polym15204121.
[19] Silveira N, Sales R, Brito C, Cândido G, Donadon M. Comparative fractographic analysis of composites adhesive joints subjected to mode I delamination. Pol Comp 2019;40(8):2973–83. https://doi.org/10.1002/pc.25139. n.d.
[20] Sales R de CM, Gusmão SR, Gouvêa RF, et al. The temperature effects on the fracture toughness of carbon fibre/RTM-6 laminates processed by VARTM. J of Comp Mat 2016;51(12):1729–41. https://doi.org/10.1177/0021998316679499.
[21] ASTM. D5573: standard practice for classifying failure Modes in fibre-reinforced-plastic (FRP) joints. West Conshohocken, PA: American Society for Testing and Materials; 2012.
[22] Fernandes R, Moura MD, Moreira R. Effect of moisture on pure Mode I and II fracture behaviour of composite bonded joints. Int J Adhesion Adhes 2016;68:30–8. https://doi.org/10.1016/j.ijadhadh.2016.01.010.
[23] KumarD S, ShuklaM J, MahatoK K, RathoreD K, PrustyR K, Ray BC. Effect of post-curing on thermal and mechanical behavior of GFRP composites. IOP Conf Ser Mater Sci Eng 2015;75:012012. https://doi.org/10.1088/1757-899X/75/1/012012.
[24] Cizmecioglu M, Gupta A, Fedors RF. Influence of cure conditions on glass transition temperature and density of an epoxy resin. J Appl Polym Sci 1986;32(8):6177–90.
[25] Apicella A, Nicolais L. Effect of water on the properties of epoxy matrix and composite. Epoxy resins and composites I, vol. 72. Berlin, Heidelberg: Springer; 1985. https://doi.org/10.1007/3-540-15546-5_3. *Adv. in Pol. Sci.*
[26] Soles C, Chang F, Bolan B, Hristov H, Gidley D, Yee A. Contributions of the nanovoid structure to the kinetics of moisture transport in epoxy resins. Polym Phys 1998;36:3035. https://doi.org/10.1002/(SICI)1099-0488(20000301)38:5<776::AID-POLB15>3.0.CO;2-A.
[27] Seymour R, Carraher CE. Polymer Chemistry. sixth ed. New York, USA: Marcel Dekker Inc; 2003.
[28] Sales R, Thim G, Brunelli D. Understanding the water uptake in F-161 glass-epoxy composites using the techniques of luminescence spectroscopy and FT-NIR *Polímeros*, vol. 27; 2017. p. 2. https://doi.org/10.1590/0104-1428.05516.
[29] Martin RH, Davidson BD. Mode II fracture toughness evaluation using four-point bend, end-notched flexure test. Plast Rub and Comps 1999;28(8):401. https://doi.org/10.1179/1465801991015405.
[30] Siddiqui NA, Woo RSC, Kim JK, Leung CKY, Munir A. Mode I Interlaminar Fracture behaviour and mechanical properties of CFRPs with Nanoclay filled epoxy matrix. Compos Appl Sci Manuf 2007;38(2):449–60. https://doi.org/10.1016/j.compositesa.2006.03.001.
[31] Yamini S, Young RJ. Mechanical properties of epoxy resins – Part 2: effect of plastic deformation on crack propagation. J of Mat Sci 1980;15(7):1823–31. https://doi.org/10.1007/BF00550603.
[32] Hunt C, Kratz J, Partridge IK. Cure path dependence of Mode I fracture toughness in interply tough thermoplastic particle prepreg laminates. Compos Appl Sci Manuf 2016;87:109–14. https://doi.org/10.1016/j.compositesa.2016.04.016.
[33] Voleppe Q, Pardoen T, Bailly C. Interdiffusion and phase separation upon curing in thermoset-thermoplastic interphases unravelled by the characterization of partially cured systems. Polymer 2016;105:120–7. https://doi.org/10.1016/J.POLYMER.2016.09.066.
[34] Sordo F, Michaud V. Adhesion and interfacial healing between supramolecular hybrid networks and glass substrates. Int J Adhesion Adhes 2017;73:100–8. https://doi.org/10.1016/J.IJADHADH.2016.11.009.
[35] Ellis B, et al. Chemistry and technology of epoxy resins. [S.l.]. Springer; 1993.
[36] Saini P. Fundamentals of conjugated polymer blends. Copolymers and composites: synthesis, properties, and Applications. [S.l.]. John Wiley & Sons; 2015.
[37] Vlasveld D, Groenewold J, Bersee H, Picken S. Moisture absorption in polyamide-6 silicate nanocomposites and its influence on the mechanical properties. Polymer 2005;46(26):12567–76. https://doi.org/10.1016/j.polymer.2005.10.096.
[38] Greenhalgh E. Failure analysis and fractography of polymer composites. Elsevier; 2009 [S.l.].
[39] Yasaee M, Bond I, Trask R, Greenhalgh E. Mode I interfacial toughening through discontinuous interleaves for damage suppression and control. Comp Part A Appl Sci and Manuf 2012;43(1):198–207. https://doi.org/10.1016/j.compositesa.2011.10.009.
[40] Xu F, Huang D-d, Du X. Improving the delamination resistance of carbon fibre/epoxy composites by brushing and abrading of the woven fabrics. Constr and Build Mat 2018;158:257–63. https://doi.org/10.1016/j.conbuildmat.2017.10.015.
[41] Purslow D. Matrix fractography of fibre-reinforced epoxy composites. Comp 1986;17(4):289–303. https://doi.org/10.1016/0010-4361(86)90746-9.
[42] Cognard P. Handbook of adhesives and sealants: general knowledge, application of adhesives, new curing techniques. [S.l.]. Elsevier; 2006.
[43] Pizzi A, Mittal KL. Handbook of adhesive technology, revised and expanded. CRC Press; 2003 [S.l.].